# Dynamics of Paired Bright Solitons Induced by the Modulational Instability of Two-component Bose-Einstein Condensates

Woo-Pyo Hong

Department of Photonics and Information Engineering, Catholic University of Daegu, Hayang, Kyongsan, Kyungbuk 712-702, South Korea

Reprint requests to Prof. W.-P. H.; E-mail: wphong@cu.ac.kr

We investigate numerically the dynamics of paired bright solitons induced by the modulational instability of two-component Bose-Einstein condensates. We derive the analytic gain spectrum by the modulational instability in terms of the interspecies and intraspecies scattering constants and classify the region where the instability occurs. The constraints on the interspecies and intraspecies scattering constants for the existence of the paired bright solitons are found. Using numerical simulations, it is shown that the paired bright solitons induced by the modulational instability exhibit complicated dynamical behaviors depending on the sign and strength of the interspecies and intraspecies scattering constants. – PACS numbers: 03.75.Fi, 05.30.Jp, 32.80Pj, 67.90.+z

*Key words:* Two-component Bose-Einstein Condensates; Modulational Instability; Paired Bright Solitons; Interaction Dynamics.

## 1. Introduction

The experimental realization of Bose-Einstein condensation (BEC) in trapped dilute alkali atom gases [1 – 3] has paved a new way to investigate various fundamental properties of quantum fluids both theoretically and experimentally. One of the most interesting achievements in the field of BEC was the experimental observation of binary mixtures of trapped condensates [4 – 8]. The species in the mixture can be atoms with different hyperfine states of the same atom [4, 5], different F-spin orientations [7, 8], or atomic-molecular BEC [9]. Several authors [10 – 16] have investigated the structure and dynamics of the interacting BECs from different perspectives.

It is expected that under interacting multicomponent BECs solitons can be formed as a result of the modulational instability (MI) which is an ubiquitous pattern-forming mechanism occuring during wave propagation in nonlinear dispersive or dissipative media, such as in fluid dynamics, in nonlinear optics, and plasma physics [17]. The recent experimental observation of matterwave bright solitons in BEC [18] has brought considerable interests for explaining the origin in connection with the MI [12, 19, 20]. The fact that two interacting BECs may generate a purely growing MI has been investigated by Timmermans [12], and was recal-
culated by Shukla et al. [19] to modify the MI gain spectrum. Recently, Carr and Brand [20] have shown that bright solitons can be formed from the MI in an attractive one-component BEC due to the s-wave scattering. More recently, Kasamatsu and Tsubota [21] have shown the multiple domain formation caused by the MI of two-component BECs in an axial symmetric trap and explained the origin of the bright soliton train observed by Miesner et al. [22].

Shukla et al. [19] have speculated that the MI-induced solitons may saturate via the formation of dispersive shock waves or nonperiodic nonlinear BEC waves by adopting the prediction by Inoue [23] in the context of two nonlinearly coupled polarized transverse waves in plasmas. However, no detailed numerical simulations have been performed to understand the behavior of MI-induced solitons yet. In particular, the dynamics of paired bright solitons of spatially homogeneous two-component BECs in the limit of vanishing trapping potential have not been investigated, which will be pursed in this work.

The paper is organized as follows: In Section 2 we derive the analytic gain spectrum of the MI in detail and investigate its dependence on the interspecies and intraspecies coupling constants. In Section 3 we find the constraints on the interspecies and intraspecies scattering constants for the existence of paired bright

solitons. We then numerically solve the coupled two-component Gross-Pitaevski equations in the limit of zero confining potential and investigate the dynamics of paired bright solitons for attractive or/and repulsive intraspecies and intraspecies scattering constants. The conclusions follow in Section 4.

## 2. The Gain by Modulational Instability

We consider the coupled Gross-Pitaevski (GP) equations for macroscopic wave functions $\psi_1$ and $\psi_2$ of interacting BECs at zero-temperature in the mean-field approximation [24, 25],

$$i\frac{\partial \psi_j}{\partial t} = \left(-\frac{1}{2}\frac{m_1}{m_j}\nabla^2 + V_j + \sum_{l=1}^{2}\lambda_{jl}|\psi_1|^2\right)\psi_j, \quad (1)$$
$$j = 1, 2,$$

where $V_j$ represents the trapping potential. These equations have been normalized to a dimensionless form by setting $\hbar = 1$ and by using $\hbar\omega_1/2$ as the energy unit and $\xi = \sqrt{\hbar/(m_1\omega_1)}$ as the length unit, where $m_j$ and $\omega_j$ denote the mass and trapping frequencies of each species, respectively. The wave functions are normalized as $\int|\psi_j|^2 d\mathbf{r} = N_j$, where $N_j$ is the number of particles of species $j$. The characteristic trap frequency $\omega_1$ is assumed to be the same for both species [10]. The dimensionless coupling constants $\lambda_{jl} = 4\pi(a_{jl}/\xi)/(m_1/\tilde{m}_{jl})$, where $\tilde{m}_{jl} = m_j m_l/(m_j + m_l)$, are related to the three scattering lengths $a_{jl}$ ($a_{12} = a_{21}$), representing the interactions between like and unlike species. In the rest of paper we denote $\lambda_{jj} = \lambda_j$ for the intraspecies constant and $\lambda_{jl} = \lambda$ ($j \neq l$) for the interspecies coupling constant. For simplicity, we consider spatially homogeneous two-component BECs with no trapping potentials for both species, i. e., $V_1 = V_2 = 0$. This means that the size of the boundary of two condensates is much smaller than that of the Thomas-Fermi radius, so that the effect of the potential on the boundary can be ignored [16, 24]. Finally, we consider the quasi-1D BEC wave function limit, so that $\psi_j(\mathbf{r}, t) = \psi_j(x, t)$ and $\nabla^2\psi_j(x, t) = \partial_{xx}\psi_j(x, t)$, as previously treated in [24, 25]. Thus, (1) can be written as

$$i\frac{\partial \psi_1}{\partial t} + \frac{1}{2}\partial_{xx}\psi_1 - \lambda_1|\psi_1|^2\psi_1 - \lambda|\psi_2|^2\psi_1 = 0,$$
$$\tag{2}$$
$$i\frac{\partial \psi_2}{\partial t} + \frac{\eta}{2}\partial_{xx}\psi_2 - \lambda_2|\psi_2|^2\psi_2 - \lambda|\psi_1|^2\psi_2 = 0,$$

where the mass ratio is defined as $\eta_{1k} = m_1/m_k$ so that $\eta_{11} = 1$ and $\eta \equiv \eta_{12}$. These equations are similar to the coupled nonlinear Schrödinger equations with the cross-phase modulation (XPM) term, which refers to the nonlinear phase change of an optical field induced by other copropagating fields in the context of fiber optics [17].

We now consider the gain by MI which can be induced by a small spatial fluctuation either by the interacting two-component boundary or by the external modulation in the form of photoassociating light applied to the atom-molecule condensate [11]. To obtain the MI gain spectrum in terms of dimensionless parameters, we introduce a slowly varying weak spatially fluctuating field $\varepsilon_j(x, t)$ to the static homogeneous condensates in equilibrium with the amplitude $|\psi_j^0|(>> |\varepsilon_j(x, t)|)$,

$$\psi_j(x, t) = [|\psi_j^{(0)}| + \varepsilon_j(x, t)]\exp[i\phi_j(t)]. \quad (3)$$

Here, the phase $\phi_j(t)$ is related to the static density of each component ($|\psi_j^{(0)}|^2 \equiv n_j$)

$$\phi_j(t) = -(\lambda_j n_j + \lambda n_{3-j})t. \quad (4)$$

By substituting (3) with (4) into (2) and linearizing in $\varepsilon_j(x, t)$, we obtain

$$i\dot{\varepsilon}_j + \frac{\eta_{1j}}{2}\varepsilon_{j,xx} - \lambda_j n_j(\varepsilon_j + \varepsilon_j^*)$$
$$- \lambda n_{3-j}^{1/2} n_j^{1/2}(\varepsilon_{3-j} + \varepsilon_{3-j}^*) = 0, \quad j = 1, 2. \quad (5)$$

We assume a general solution of the form

$$\varepsilon_j = u_j\cos(Kx - \Omega_k t) + i v_j\sin(Kx - \Omega_k t), \quad (6)$$

where $K$ and $\Omega_k$ are the normalized dimensionless wavenumber and the frequency of modulation, respectively. After substituting this general solution into (5), we require the determinant of the subsequent four homogeneous equations for $u_1$, $u_2$, $v_1$, and $v_2$ to be zero, which yields a nonlinear dispersion relation as

$$(\Omega_k^2 - E_1)(\Omega_k^2 - E_2) = X^2, \quad (7)$$

where

$$E_1 = \frac{1}{4}K^2(K^2 + 4\lambda_1 n_1), \quad E_2 = \frac{1}{4}\eta K^2(\eta K^2 + 4\lambda_2 n_2),$$
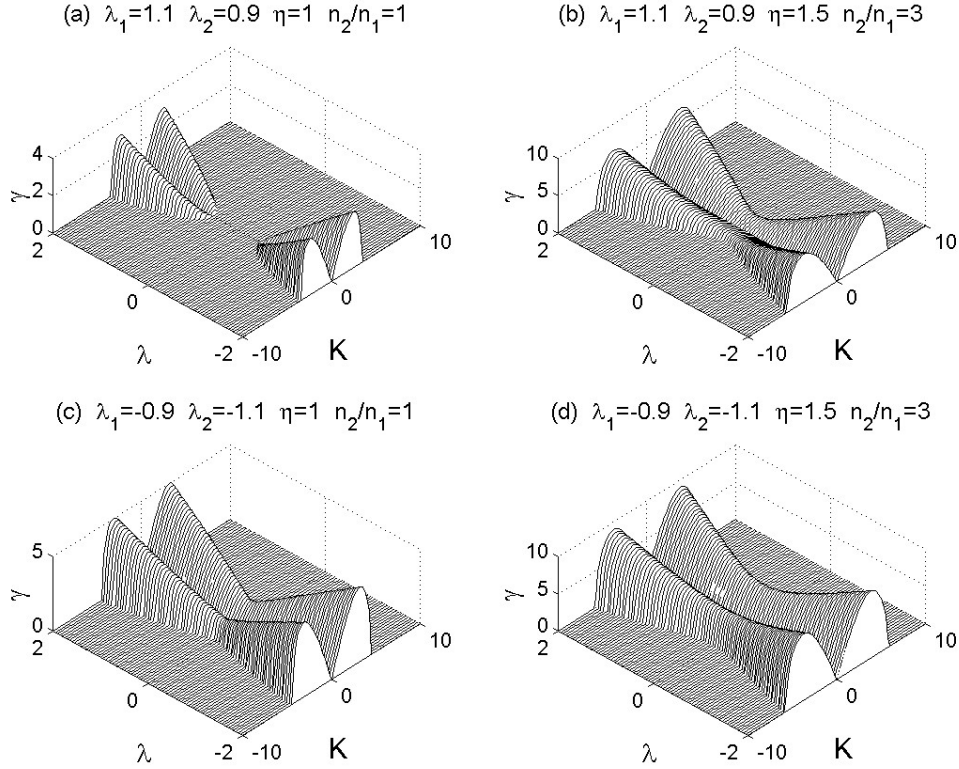
$$X^2 = \lambda^2 n_1 n_2 \eta K^4. \quad (8)$$

Fig. 1. The MI gain spectra as functions of the interspecies coupling constant $\lambda$ and the wavenumber $K$ for several values of the intraspecies coupling constants $\lambda_1$ and $\lambda_2$, the mass ratio $\eta$, and the ratio of the static number densities $n_2/n_1$. (a, b) The gain plots for the attractive intraspecies coupling constants. The gain in (a) vanishes for $\lambda$ in the region $-\sqrt{\lambda_1\lambda_2} < \lambda < \sqrt{\lambda_1\lambda_2}$. As the mass ratio and the density ratio increase, the gain does not vanish in the absence of the interspecies coupling constant, as shown in (b). (c, d) The gain spectra for the repulsive intraspecies coupling constants. The magnitude and width of the gain spectrum grow with increasing mass and density ratio in comparison of (c) with (d).

These equations agree with the expressions obtained in [19] expected for the ratio of the two atoms $\eta$. We observe from (7) that in the absence of the interspecies interaction, i.e., $X = 0$, the modulation frequencies $\Omega_k = \pm\sqrt{E_j}(j = 1,2)$ are always real for $^{87}$Rb or $^{23}$Na atoms due to repulsive intraspecies s-wave scattering: the system is modulationally stable. However, for a BEC consisting of $^7$Li or $^{85}$Rb atoms with attractive s-wave scattering, the system can be modulationally unstable since the frequency can be purely imaginary, i.e., $\Omega_k = i|\sqrt{E_j}|$, depending on the magnitude of the static BEC density and the intraspecies coupling constant, which has not been mentioned in the previous work [19]. A more complicated MI gain spectrum for the two-component BECs system in the presence of both interspecies and intraspecies scatterings, i.e., $X \neq 0$, is expected. We define the purely growing MI gain (viz. $\Omega_k = i\gamma$ where $\gamma > 0$) as

$$\gamma = \left[ -\frac{1}{2}(E_2 + E_1) + \frac{1}{2}\sqrt{(E_2 + E_1)^2 + 4(X^2 - E_1E_2)} \right]^{1/2}, \tag{9}$$

which agrees with the result in [19] for $\eta = 1$. Obviously, the gain is real if the condition $X^2 > E_1E_2$ is satisfied for some specific values of $K$, i.e.,

$$K^2 < \frac{-2\lambda_2 n_2 - 2\eta\lambda_1 n_1 + 2\sqrt{(\lambda_2 n_2 - \eta\lambda_1 n_1)^2 + 4\lambda^2 n_2 n_1 \eta}}{\eta}. \tag{10}$$

We plot in Fig. 1 the MI gain spectrum $\gamma$ as functions of $\lambda$ and $K$, respectively, for some repulsive and attractive intraspecies coupling constants. They show characteristic dependences in the ranges of the parameters, such as the coupling constants, the mass ratio, and the static number density. In particular, it is interesting to note in Fig. 1a that even in the presence of nonzero interspecies scattering, as long as the coupling constant is in the region $-\sqrt{\lambda_1 \lambda_2} < \lambda < \sqrt{\lambda_1 \lambda_2}$, the gain vanishes. On the other hand, as shown in Fig. 1b, the gain is not only nonzero for the case of $\lambda = 0$ but also it increases with higher $\eta$ and $n_2/n_1$, in comparison with Figure 1a. We observe in Fig. 1c that for attractive intraspecies coupling constants the gain does not vanish at $\lambda = 0$ in contrast with Fig. 1a. Furthermore, it is also shown in Fig. 1d that the magnitude and width of the gain spectrum grow with increasing mass and density ratio. From these, we conclude that two-component BECs can be modulationally unstable regardless of the presence or the absence of the interspecies coupling constant due to the MI gain's dependence on the strength of the intraspecies coupling constants, the mass ratio, and the static number density ratio.

In an experimentally accessible two-component BECs system, such as the mixture of $^{87}$Rb$|1,-1>$ and $^{85}$Rb$|2,2>$, it has been demonstrated that one can control the ratio of the intraspecies and interspecies coupling constants in the range of $0 < \lambda_1 \lambda_2/\lambda^2 < 1$ by applying a bias magnetic field and taking advantage of Feshbach resonances [26,27]. Thus it maybe interesting to investigate the dynamics of bright solitons induced by the MI from the initial static densities for the range of interspecies and intraspecies coupling constants experimentally accessible now or in the future.

## 3. Dynamics of Paired Bright BEC Solitons

In order to understand the dynamics of the bright solitons induced by the MI, we numerically solve (2), utilizing the split-step Fourier method taking the Crank-Nicholson implicit scheme for time propagation under periodic boundary conditions [28]. In the following analysis we investigate the effects of the interspecies and intraspecies coupling constants on the dynamics of the bright solitons in the nonlinear regime. In our numerical simulations we take the initial static number densities as

$$\psi_j(x,0) = \sqrt{n_{j0}}[1 + \varepsilon_0 \cos(Kx)], \qquad (11)$$

where $\varepsilon_0$ is the small amplitude of spatial excitation to start the MI, which may originate from an artificially applied external noise [11] or the self-interference of the BEC [20]. In the following we fix $\varepsilon_0 = 0.01$ and the wavenumber $K = 1$, and the initial static densities for both atoms as $n_{j0} = 1$ for the sake of numerical computations.

Before going further, we would like to know the types of solitons allowed in (2). It is well-known in the context of nonlinear optics that the coupled nonlinear Schrödinger equations with the XPM terms possess bright-dark, bright-bright, and bright-gray paired solitons, preserving their shapes through the mutual interaction [28]. Thus we expect to find similar paired soliton solutions depending on the interspecies and intraspecies coupling constants. The conditions for the existence of bright soliton pairs can be sought by solving (2) with the ansatz $\psi_j(x,t) = Q_j(t - x/v) \exp[i(k_j x - \omega_j t)]$, where $Q_j$ denotes a real soliton shape function, $k_j$ and $\omega_j$ represent the dimensionless propagation constant and the frequency of the soliton pairs, respectively. After some algebraic steps, we find the solutions in the form

$$Q_1 = B_1 \operatorname{sech}(W\tau), \quad Q_2 = B_2 \operatorname{sech}(W\tau), \quad (12)$$

where $\tau = t - x/v$ and $W$ is the pulse width. The soliton amplitudes can be found as

$$B_1^2 = \frac{W^2}{v^2} \frac{\lambda_2 - \eta\lambda}{\lambda^2 - \lambda_1\lambda_2}, \quad B_2^2 = \frac{W^2}{v^2} \frac{\eta\lambda_1 - \lambda}{\lambda^2 - \lambda_1\lambda_2}. \quad (13)$$

The requirement for real amplitudes, i.e., $B_1^2 > 0$ and $B_2^2 > 0$, can yield some constraints for the paired bright solitons. For simplicity we set the mass ratio $\eta = 1$. Firstly, by considering the case of both the numerator and denominator $B_1^2$ and $B_2^2$ being positive, we find

$$\lambda < \lambda_1 \text{ and } \lambda < \lambda_2 \text{ and } \lambda < -\sqrt{\lambda_1\lambda_2}, \qquad (14)$$

which are the constraints for the paired bright solitons. Secondly, for the case of both the numerator and denominator of $B_1^2$ and $B_2^2$ being negative, we find

$$\lambda > \lambda_1 \text{ and } \lambda > \lambda_2 \text{ and } -\sqrt{\lambda_1\lambda_2} < \lambda < \sqrt{\lambda_1\lambda_2}, \quad (15)$$

which yield $0 \le \lambda < 1$ while $\lambda_1 \le -1$ and $\lambda_2 \le -1$. Possible sets of the interspecies and intraspecies coupling constants for the paired bright solitons can be diverse according to (13). For the above cases in (14)–(15), we have run extensive simulations to find the following results.
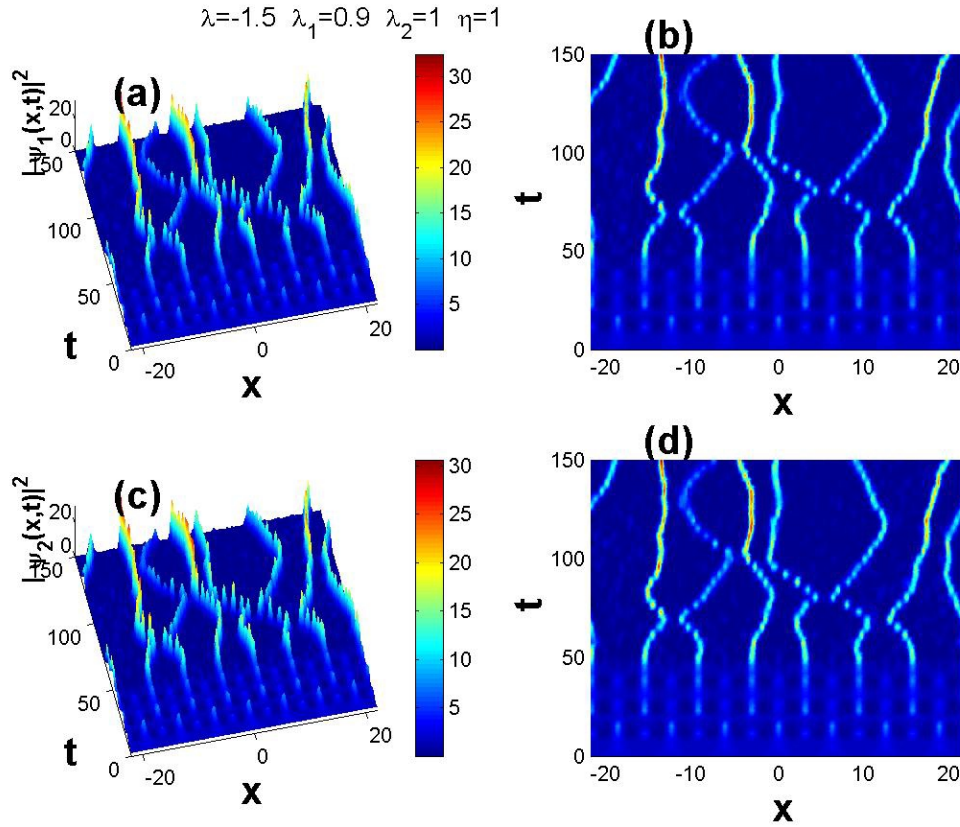
Fig. 2. Evolutions of paired bright solitons for an attractive interspecies coupling constant satisfying $\lambda < -\sqrt{\lambda_1 \lambda_2}$. The wavenumber $K = 1$ is so chosen that the MI initially produces seven density peaks. (a) and (b) are plots of $|\psi_1(x,t)|^2$ and its contour, respectively. Attractive and repulsive interactions (scatterings) between the solitons are shown. (c) and (d) are plots of $|\psi_2(x,t)|^2$ and its contour, respectively. The evolution of the second atom shows an identical dynamical pattern as (a).

### 3.1. Attractive Interspecies Scattering: $\lambda < -\sqrt{\lambda_1 \lambda_2}$

We consider the effects of the attractive interspecies scattering on the evolution of initial static condensates. Figures 2a and b show the evolution of the density $|\psi_1(x,t)|^2$ and its corresponding contour plot, respectively, for the attractive interspecies and repulsive intraspecies coupling constants. We set the range of $x$ such that the initial MI produces seven initial density peaks for the wavenumber value $K = 1$. Evidently the initial static density grows due to the MI to form the soliton trains by showing complicated interaction patterns: Firstly, the solitons show the breathing behavior before and after their mutual interactions as demonstrated in Figure 2a. Secondly, the solitons scatter each other for example at $t \approx 70$ and at $t \approx 100$, after which similar patterns are repeated. Lastly, the peak densities of the solitons increase with time. An intuitive

explanation for the increasing density peak is that a small amplitude initial soliton, once formed by the MI, can only become more and more localized due to the strong interspecies coupling constant terms in (2). Subsequently, the MI with strong nonlinearity produces a more localized density peak with large amplitude. This result is similar to the behavior of the bright soliton train induced by the MI for the single BEC with only attractive s-wave scattering between the atoms [20]. As shown in Figs. 2c and 2d for the evolution of the density $|\psi_2(x,t)|^2$ and its corresponding contour plot, respectively, we find a similar interaction pattern as the first atoms. This can be understood, since once the solitons form their dynamics are governed by (2) in which the interspecies coupling terms dominate over those of the intraspecies. It should be mentioned that although all the simulations are shown up to $t = 150$ in Fig. 2, the similar dynamics has been checked to continue up
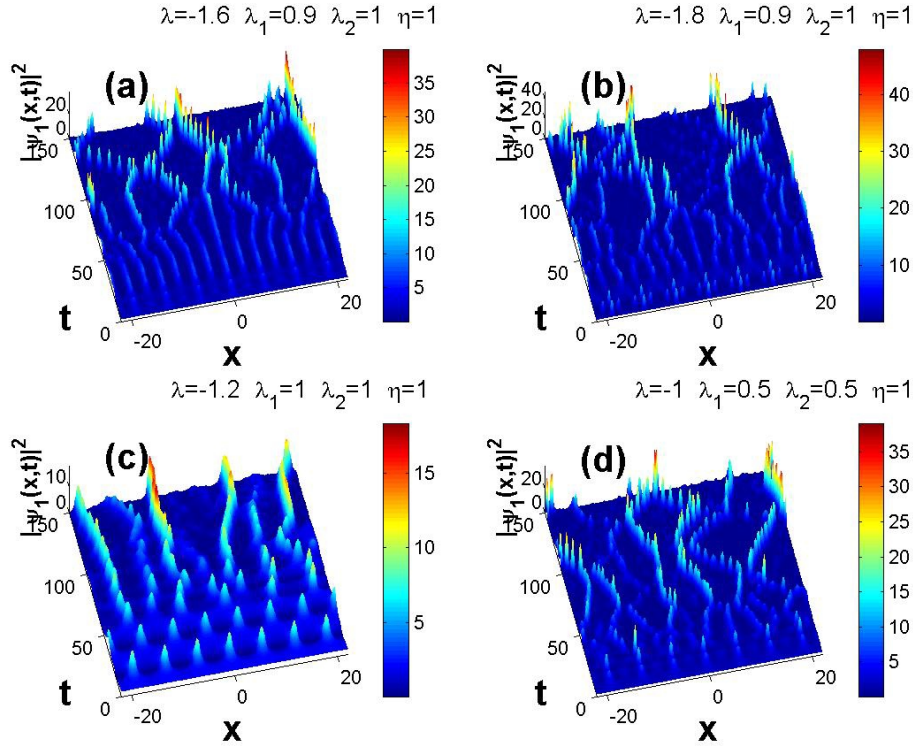
Fig. 3. Evolutions of bright solitons for different attractive interspecies coupling constants. (a) and (b) are plots of $|\psi_1(x,t)|^2$ for strong interspecies coupling constants. Too strong interspecies coupling constants result in suppression of soliton formation, reduction of mutual interaction, and increase of the peak soliton density. (c) and (d) are plots of $|\psi_1(x,t)|^2$ for weak interspecies coupling constants. The recurrences of solitons induced by MI are shown in (c). The trains of solitons propagate without mutual scattering. (d) For both weak interspecies and intraspecies coupling constants, a similar interaction pattern as shown in (a) appears.

to $t = 300$. The dynamical patterns shown here resemble the evolution of the atomic and molecular condensates in equilibrium in the presence of photoassociating light [11].

In order to further elaborate the effects of the interspecies scattering, we present the simulation results for stronger coupling constants in Figs. 3a and b and for weaker coupling constants in Fig. 3c and d, respectively. Figure 3a, for slightly stronger $\lambda$ in comparison with Fig. 2, shows more scatterings between the solitons at $t \approx 120$, after which they breathe during the propagation. The reason is that the strength of the interspecies terms in (1) dominate over the intraspecies terms. However, when the interspecies coupling gets too strong, as shown in Fig. 3b, we find suppression of soliton formation by the MI, reduction of mutual interaction between the solitons, and increase of peak density. On the other hand, for the weaker interspecies coupling constant in Fig. 3c, we observe the recur-

rences of the MI induced solitons up to $t \approx 75$, after which they show stable propagation in the form of soliton trains without having mutual interactions. Finally, for further the reduced interspecies and intraspecies coupling constants in Fig. 3d, we observe overall the similar dynamical pattern as in Figure 3a. Lastly, it is worth mentioning that according to the constraint in (14) $\lambda_1 < 0$ and $\lambda_2 < 0$ are allowed for the paired bright solitons. However, for several different sets of the attractive intraspecies coupling constants, we have run simulations to find that the bright solitons initially induced by the MI quickly enter to chaotic states or decay to dispersive waves.

## 3.2. Repulsive Interspecies Scattering: $0 \leq \lambda < 1$

The constraints for the paired bright solitons in (15), i.e., $0 \leq \lambda < 1$ while $\lambda_1 \leq -1$ and $\lambda_2 \leq -1$, requier weaker repulsive interspecies coupling constants than
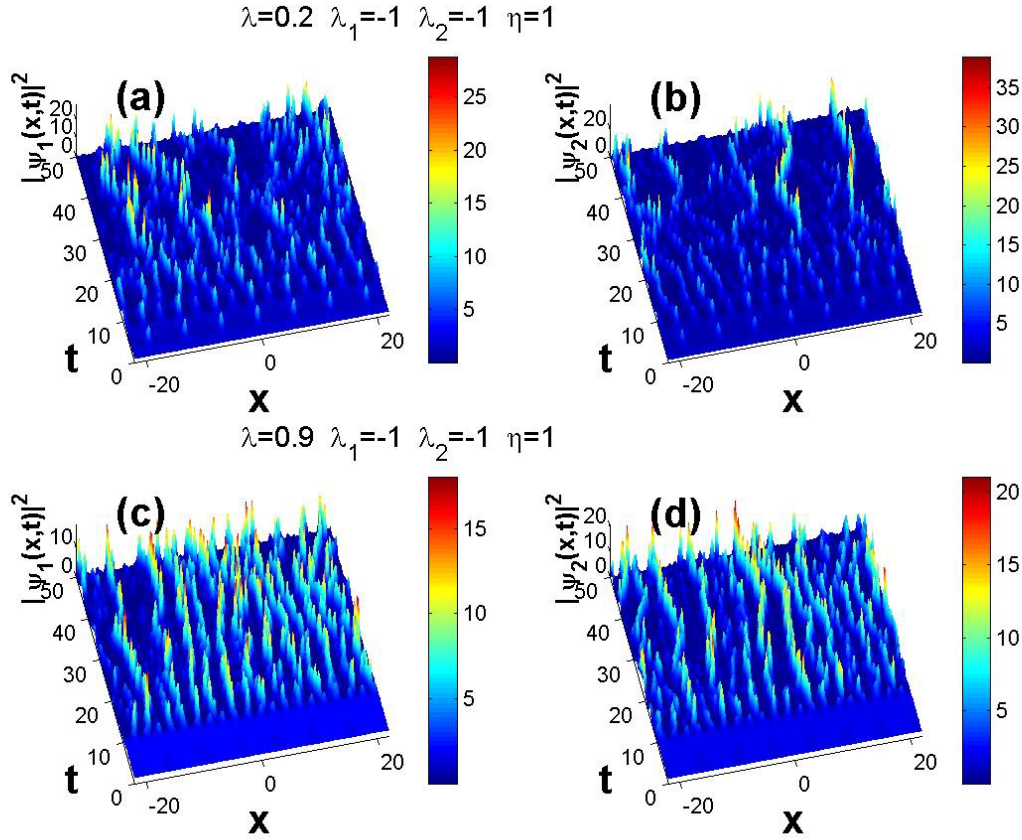
Fig. 4. Evolutions of bright solitons for different repulsive interspecies coupling constants. (a) and (b) show plots of $|\psi_1(x,t)|^2$ and $|\psi_1(x,t)|^2$ for $\lambda = 0.2$, respectively. The dynamics of the two condensates are not identical. The interaction between the solitons is suppressed and the dynamics are similar to Fig. 3c except that the intensities of the solitons increase and exhibit a breather-like behavior. (c) and (d) are plots of $|\psi_1(x,t)|^2$ and $|\psi_1(x,t)|^2$, respectively, for $\lambda = 0.9$. The trains of the solitons form and interact weakly at $t \approx 40$, after which they show stable propagations.

the intraspecies coupling constants. Figure 4 shows the evolutions of the two condensates for different interspecies coupling constants. In contrast to Figs. 2 and 3, the dynamics of the two condensates are not identical, as shown in Figs. 4a and b for $\lambda = 0.2$ and Figs. 4c and d for $\lambda = 0.9$, respectively. The reason is, that under weakly repulsive interspecies interaction, once the solitons are induced by the MI, their evolutions are governed by (2), where the intraspecies terms dominate over the interspecies terms, which still influence the dynamics. Actually, in the limit of $\lambda \to 0$ with $\lambda_1 \leq -1$ and $\lambda_2 \leq -1$, we confirmed that the two condensates form exactly the same bright soliton trains, as expected, since the gain is nonzero according to Figs. 1c and d. In Figs. 4a and b, we observe that the interaction between the solitons is suppressed, of

which the dynamics are similar to Fig. 3c except that the intensities of the solitons increase and they exhibit a breather-like behavior. For stronger interspecies coupling constant in Figs. 4c and d, the trains of solitons initially form and interact weakly at $t \approx 40$, after which they show stable propagations.

## 4. Conclusions

In this work we have obtained the gain spectrum of interacting two-component Bose-Einstein condensates in (9) as functions of the interspecies and the intraspecies coupling constants, the static number density ratio, and the mass ratio of two condensates. We have found that the two-component BECs can be modulationally unstable regardless of the presence or the

absence of the interspecies coupling constant due to the MI gain's dependence on the strength of the intraspecies coupling constants, the mass ratio, and the static number density ratio.

We have classified the allowed interspecies and intraspecies coupling constants for the existence of the paired bright BEC solitons in (14) and (15). For an attractive interspecies scattering, $\lambda < \lambda_1$ and $\lambda < \lambda_2$ and $\lambda < -\sqrt{\lambda_1\lambda_2}$ should be satisfied. For an repulsive interspecies scattering, $\lambda > \lambda_1$ and $\lambda > \lambda_2$ and $-\sqrt{\lambda_1\lambda_2} < \lambda < \sqrt{\lambda_1\lambda_2}$ should be satisfied. Motivated by the fact that one can control the ratio of the intraspecies and interspecies coupling constants in the range of $0 < \lambda_1\lambda_2/\lambda^2 < 1$ by applying a bias magnetic field and taking advantage of Feshbach resonances [26, 27], we have investigated the evolutions of the paired bright solitons induced by the MI using numerical simulations to find complex dynamical behavior as demonstrated in Figs. $2-4$. Contrary to the previous predictions that the modulationally unstable condensates might saturate via the formation of dispersive shock waves or nonperiodic nonlinear BEC wave trains, as predicted by Inoue [23] in the context of two nonlinearly coupled polarized transverse waves in plasmas [19], we have observed that for the case of the attractive interspecies coupling constant in Fig. 3 the paired solitons form from the initial static densities by the MI and show stable propagation while having strong mutual scatterings. As demonstrated in Fig. 4, for the repulsive interspecies coupling constants, trains of solitons can also form with breather-like behavior by showing weak attractive scattering between the solitons. From these, we conclude that for the interspecies and intraspecies coupling constants experimentally accessible now or in the future one may find some interesting soliton dynamics of the two-component Bose-Einstein condensates described by (2).

*Acknowledgement*

[1] M. H. Anderson, J. R. Ensher, M. R. Matthews, C. E. Wieman, and E. A. Cornell, Science **269**, 1989 (1995).

[2] K. B. Davis, M.-O. Mewes, M. R. Andrews, N. J. van Druten, D. S. Durfee, D. M. Kurn, and W. Ketterle, Phys. Rev. Lett. **75**, 3969 (1995).

[3] C. C. Bradley, C. A. Sackett, and R. G. Hulet, Phys. Rev. Lett. **78**, 985 (1997).

[4] C. J. Myatt, E. A. Burt, W. Ghirst, E. A. Cornell, and C. E. Wieman, Phys. Rev. Lett. **78**, 586 (1997).

[5] D. S. Hall, M. R. Matthews, J. R. Ensher, C. E. Wieman, and E. A. Cornell, Phys. Rev. Lett. **81**, 1539 (1998).

[6] D. S. Hall, M. R. Matthews, C. E. Wieman, and E. A. Cornell, Phys. Rev. Lett. **81**, 1543 (1998).

[7] D. M. Stamper-Kurn, A. P. Chikkatur, A. Görlitz, S. Inouye, S. Gupta, D. E. Pritchard, and W. Ketterle, Phys. Rev. Lett. **83**, 2072 (1998).

[8] J. Stenger, S. Inouye, M. R. Andrews, H.-J. Miesner, D. M. Stamper-Kurn, and W. Ketterle, Phys. Rev. Lett. **82**, 4569 (1999).

[9] R. Wynar, R. S. Freeland, D. J. Han, C. Ryu, and D. J. Heinzen, Science **287**, 1016 (2000).

[10] B. J. Cusack, T. J. Alexander, E. A. Ostrovskaya, and Y. S. Kivshar Phys. Rev. A **65**, 013609 (2001).

[11] J. Javanainen and M. Koštrun, Opt. Express **5**, 188 (1999).

[12] E. Timmermans, Phys. Rev. Lett. **81**, 5718 (1998).

[13] P. Ao and S. T. Chui, Phys. Rev. A **58**, 4836 (1998).

[14] H. Pu and N. P. Bigelow, Phys. Rev. Lett. **80**, 1134 (1998).

[15] H. Shi, W.-M. Zheng, and S.-T. Chui, Phys. Rev. A **61**, 063613 (2000).

[16] R. A. Barankov, Phys. Rev. A **66**, 013612 (2002).

[17] G. P. Agrawal, Phys. Rev. Lett. **59**, 880 (1997) and references therein.

[18] K. E. Strecker, G. B. Patridge, A. G. Truscott, and R. G. Hulet, Nature **417**, 150 (2002).

[19] P. K. Shukla, L. Stenflo, and R. Fedele, Phys. Scr. **64**, 113 (2001).

[20] L. D. Carr and J. Brand, Phys. Rev. Lett. **92**, 040401 (2004).

[21] K. Kasamatsu and M. Tsubota, Phys. Rev. Lett. **93**, 100402 (2004).

[22] H. J. Miesner, D. M. Stamper-Kurn, J. Stenger, S. Inouye, A. P. Chikkatur, and W. Ketterle, Phys. Rev. Lett. **82**, 2228 (1999).

[23] Y. J. Inoue, J. Plasma Phys. **16**, 439 (1976).

[24] S. Coen and M. Haelterman, Phys. Rev. Lett. **87**, 140401 (2001).

[25] Th. Busch and J. R. Anglin, Phys. Rev. Lett. **87**, 010401 (2001).

[26] L. Salasnich, A. Parola, and L. Reatto, Phys. Rev. Lett. **91**, 080405 (2003).

[27] S. Inouye, M. R. Andrews, J. Stenger, H.-J. Miesner, D. M. Stamper-Kurn, and W. Ketterle, Nature **392**, 151 (1998).

[28] G. P. Agrawal, Nonlinear Fiber Optics, Optics and Photonics, Academic Press, 3rd. ed., New York 2001, and references therein.